BIOCHEMISTRY
including biophysical chemistry & molecular biology

New Concept

pubs.acs.org/biochemistry

Interpretation of pH–Activity Profiles for Acid–Base Catalysis from Molecular Simulations

Thakshila Dissanayake,[†] Jason M. Swails,[†] Michael E. Harris,[‡] Adrian E. Roitberg,[§] and Darrin M. York*[,†]

[†]Center for Integrative Proteomics Research, BioMaPS Institute, and Department of Chemistry & Chemical Biology, Rutgers University, 174 Frelinghuysen Road, Piscataway, New Jersey 08854-8076, United States

[‡]Department of Biochemistry, Case Western Reserve University School of Medicine, Cleveland, Ohio 44106, United States

[§]Quantum Theory Project, Chemistry Department, University of Florida, Gainesville, Florida 32611, United States

Supporting Information

ABSTRACT: The measurement of reaction rate as a function of pH provides essential information about mechanism. These rates are sensitive to the pK_a values of amino acids directly involved in catalysis that are often shifted by the enzyme active site environment. Experimentally observed pH–rate profiles are usually interpreted using simple kinetic models that allow estimation of "apparent pK_a" values of presumed general acid and base catalysts. One of the underlying assumptions in these models is that the protonation states are uncorrelated. In this work, we introduce the use of constant pH molecular dynamics simulations in explicit solvent (CpHMD) with replica exchange in the pH-dimension (pH-REMD) as a tool to aid in the interpretation of pH–activity data of enzymes and to test the validity of different kinetic models. We apply the methods to RNase A, a prototype acid–base catalyst, to predict the macroscopic and microscopic pK_a values, as well as the shape of the pH–rate profile. Results for apo and cCMP-bound RNase A agree well with available experimental data and suggest that deprotonation of the general acid and protonation of the general base are not strongly coupled in transphosphorylation and hydrolysis steps. Stronger coupling, however, is predicted for the Lys41 and His119 protonation states in apo RNase A, leading to the requirement for a microscopic kinetic model. This type of analysis may be important for other catalytic systems where the active forms of the implicated general acid and base are oppositely charged and more highly correlated. These results suggest a new way for CpHMD/pH-REMD simulations to bridge the gap with experiments to provide a molecular-level interpretation of pH–activity data in studies of enzyme mechanisms.

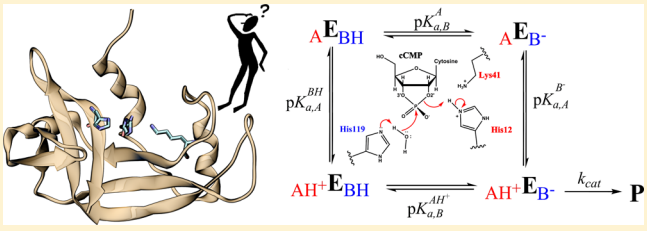

Acid–base catalysis is a common catalytic strategy in protein and RNA enzymes[1] and is employed in the cleavage of the RNA phosphodiester backbone by RNase A[2,3] as well as small nucleolytic RNA enzymes.[4] General base and acid catalysts facilitate nucleophile activation through proton abstraction and promote leaving group departure through proton donation, respectively. The observed reaction rate is assumed to be proportional to the probability of finding the enzyme in a "catalytically active" state with the acid protonated (i.e., able to donate a proton) and the base deprotonated (i.e., able to receive a proton). This conditional probability will thus be a function of the pH, and the pH–rate curves will be sensitive to the pK_a values of the general acid and base.[5,6]

The measurement of reaction kinetics as a function of pH provides vital information about mechanism; however, the interpretation of this data is not always straightforward.[6] Experimentally determined pH–rate curves are commonly fit to a simple equilibrium model in which the apparent pK_a values of the general acid and base appear as independent parameters. When protonation states are strongly coupled as they often are in enzyme active sites, irregular titration behavior occurs, requiring a more detailed theoretical analysis.[5,7,8] Recently, computational methods have emerged that allow molecular simulations in explicit solvent to be performed under constant pH conditions (CpHMD), and the conditional probabilities of correlated protonation events to be directly determined.[9−16] CpHMD can be used in conjunction with replica exchange molecular dynamics in the pH-dimension (pH-REMD) to enhance sampling of important states while at the same time providing information over a range of pH values that can be used to predict complex titration curves.[9,17] This work reports the first application of the CpHMD/pH-REMD method to the prediction of the pH–rate curves for the apo and 2′,3′-cyclic phosphate (2′-O-transphosphorylation product)-bound RNase A, a prototype acid–base catalyst.

RNase A catalyzes a 2′-O-transphosphorylation of a bound RNA substrate that involves cleavage of the phosphodiester backbone to form a 2′,3′-cyclic phosphate and 5′-hydroxyl termini.[2,3] In a subsequent reaction, RNase A catalyzes the hydrolysis of the cyclic phosphate to form a 3′-phosphate. Both transphosphorylation and hydrolysis involve general acid–base catalysis and thus are strongly pH-dependent. The kinetics of

Received: October 13, 2014
Revised: January 13, 2015
Published: January 23, 2015

DOI: 10.1021/bi5012833
Biochemistry 2015, 54, 1307−1313

Scheme 1. Putative Mechanism of Transphosphorylation (left) and Hydrolysis (right) by RNase A[a]

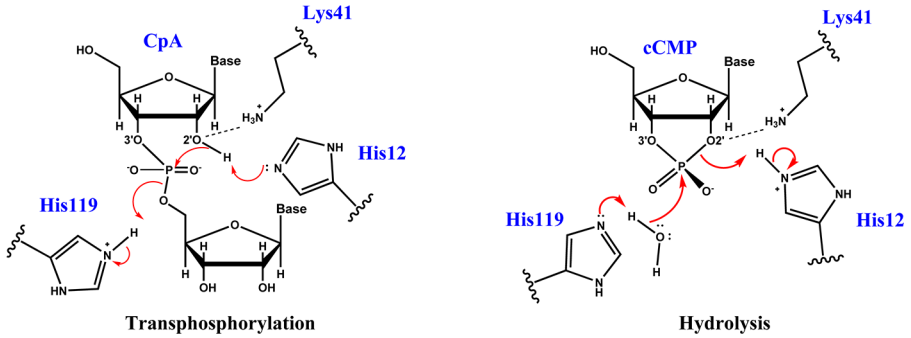

[a]The generally accepted view is that the H119/H12 pair acts as the general acid/base pair in transphosphorylation, and their roles are reversed in hydrolysis. However, there has been some debate in the literature that, alternatively, K41 might act as general base in transphosphorylation, although this is less widely accepted.

RNase A have been extensively studied,[18,19] including analysis of the roles of His12 and His119[20] and the pH dependence of substrate association.[21] In this work, we examine the effect of pH on the acid–base catalytic step in RNase A 2′-O-transphosphorylation and hydrolysis. We do not consider here the effect of pH on substrate association and binding, which is known to be important.[21] Extension of the theoretical framework to take into account the added dimension of substrate binding is possible, but this requires technical details that are beyond the scope of this first application. Nonetheless, we note that very recent progress in this area has been reported.[22]

Scheme 1 illustrates the putative mechanism of RNA cleavage via transphosphorylation and hydrolysis of cytidyl-3′,5′-adenosine (CpA) and 2′,3′-cyclic phosphate by RNase A.[2,3] The His119/His12 pair is a generally accepted general acid/base pair in transphosphorylation (although other mechanisms have been proposed and discussed[3]). His12 abstracts the proton from O2′ to facilitate the nucleophilic attack on the adjacent phosphorus atom. His119 act as the general acid to donate a proton to the O5′ leaving group, resulting in a 2′,3′-cyclic phosphate. Subsequent hydrolysis occurs by the action of His119 as the general base to abstract the proton from a water molecule to facilitate nucleophilic attack. The His12 residue acts as the general acid to donate a proton to O2′ and leads to the 3′-phosphomonoester final product. Note that some reports in the literature[23,24] have suggested that Lys41, rather than His12, may play the role of the general base in transphosphorylation. Although this mechanism is not widely accepted, we nonetheless consider it for comparison.

METHODS

Interpretation of pH–Rate Data for General Acid–Base Catalysis. Scheme 2 illustrates a microscopic kinetic model for general acid–base catalysis used to interpret pH–activity data. The underlying kinetic assumption is that the catalytic rate is proportional to the active species, $_{AH^+}E_{B^-}$, which has the general base deprotonated (B^-) so that it can accept a proton and activate the nucleophile, while the general acid (AH^+) is protonated so that it can donate a proton to the leaving group.

The pH-dependent probabilities for each of the four microstates illustrated in Scheme 2 can be described by the partition function Q

Scheme 2. Microscopic General Acid–Base Protonation State Model Used To Interpret pH–Activity Data[a]

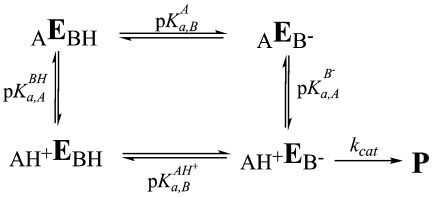

[a]$_{AH^+}E_{B^-}$, $_{AH^+}E_{BH}$, $_{A}E_{BH}$, and $_{A}E_{B^-}$ are four microstates. E stands for "enzyme", and subscripts A and B indicate the acid and base, respectively. The pK_a shifts discussed in the text are defined as $\Delta pK_{a,A} = pK_{a,A}^{BH} - pK_{a,A}^{B^-}$ and $\Delta pK_{a,B} = pK_{a,B}^{A} - pK_{a,B}^{AH^+}$. Note the constraint of the thermodynamic cycle ensures $\Delta pK_{a,A} + \Delta pK_{a,B} = 0$; a positive value for $\Delta pK_{a,B}$ indicates anticooperative coupling of protonation states (i.e., protonation of the acid site disfavors protonation of the base), whereas a negative value of $\Delta pK_{a,B}$ indicates cooperative coupling (i.e., protonation of the acid site favors protonation of the base). The "apparent pK_a" model discussed in the text involves fitting of pH–rate data under the constraint that $\Delta pK_{a,A} = -\Delta pK_{a,B} = 0$ (see the text). This scheme does not consider the pH dependence of substrate binding, which is also important for a complete kinetic characterization.

$$Q = 1 + 10^{pK_{a,B}^{AH^+} - pH} + 10^{pK_{a,B}^{AH^+} - pK_{a,A}^{BH}} + 10^{pH - pK_{a,A}^{B^-}} \quad (1)$$

from which the probabilities (fractions) for each state can be determined as

$$f_{(AH^+/B^-)} = 1/Q \quad (2)$$

$$f_{(AH^+/BH)} = 10^{pK_{a,B}^{AH^+} - pH}/Q \quad (3)$$

$$f_{(A/BH)} = 10^{pK_{a,B}^{AH^+} - pK_{a,A}^{BH}}/Q \quad (4)$$

$$f_{(A/B^-)} = 10^{pH - pK_{a,A}^{B^-}}/Q \quad (5)$$

Note that the reference energy in the partition function is taken as that of the active state $_{AH^+}E_{B^-}$ (set to zero energy). The microscopic pK_a values can be determined from fitting to these four fractions simultaneously under the constraint that their related free energy values sum to zero in accord with the thermodynamic cycle shown in Scheme 2. The plots of the data used in deriving microscopic pK_a values can be found in the Supporting Information.

DOI: 10.1021/bi5012833
Biochemistry 2015, 54, 1307–1313

A common assumption in the interpretation of pH−rate profiles is that the protonation/deprotonation events are uncorrelated; i.e., an equivalence is assumed between microscopic pK_a values [$pK_{a,A}^{BH} = pK_{a,A}^{B^-}$ and $pK_{a,B}^{AH^+} = pK_{a,B}^{A}$, or equivalently $\Delta pK_{a,A} = -\Delta pK_{a,B} = 0$, where $\Delta pK_{a,A} = pK_{a,A}^{BH} - pK_{a,A}^{B^-}$ and $\Delta pK_{a,B} = pK_{a,B}^{A} - pK_{a,B}^{AH^+}$ (for a more complete discussion, see ref 6)]. Fitting of the pH−rate data under these constraints leads to apparent pK_a values for the general acid and base, and we will henceforth refer to this model as the "apparent pK_a model" to distinguish it from the "microscopic pK_a model" that allows this coupling parameter to be optimized. Alternatively, direct determination of the macroscopic pK_a values of the individual acid and base sites involves fitting to each of the corresponding independent acid and base fractions

$$f_{(AH^+)} = f_{(AH^+/BH)} + f_{(AH^+/B^-)} \quad (6)$$

$$f_{(B^-)} = f_{(A/B^-)} + f_{(AH^+/B^-)} \quad (7)$$

using the Hill equation

$$f_{(d)} = 1/[1 + 10^{n(pK_a - pH)}] \quad (8)$$

where $f_{(d)}$ is the deprotonated fraction of the residue of interest [either $f_{(AH)}$ or $f_{(B^-)}$] and n is the Hill coefficient.

Molecular Dynamics Simulations at Constant pH. The starting structures for the simulations were prepared by modifying the crystallographic structure of apo RNase A (Protein Data Bank entry 1KF5)[25] and RNase A complexed with deoxycytidyl-3′,5′-deoxyadenosine [d(CpA)] (Protein Data Bank entry 1RPG)[26] determined at 1.15 and 1.4 Å resolution, respectively. Two separate sets of explicit solvent constant pH replica exchange molecular dynamics (CpHMD/pH-REMD)[9] simulations were performed using a developmental version of the Amber 12[27] molecular dynamics package on apo RNase A and the product state, 2′,3′-cyclic phosphate (cCMP)-bound RNase A. The apo and complexed RNase A structures were each placed in a cubic box of TIP4P-Ew[28] water molecules having a buffer of at least 10 Å on each side and neutralized by chloride counterions for the expected charge of the systems (standard amino acid protonation states) at pH 7 with the exception of His12 and His119 treated as fully protonated. Note that the net number of explicit ions is constant in all the simulations, so the net charge of the system does vary as titratable residues undergo changes in protonation state. This point was addressed specifically with regard to the titration process in ref 9 and shown not to affect the titration because the sampling of protonation states occurs using an implicit solvent model based on the conformations generated with explicit solvent simulation. After initial minimization and equilibration with molecular dynamics, pH-REMD simulations in explicit solvent[9] were performed at 300 K and 1 bar using a total of 24 replicas corresponding to different pH values between 2 and 13. During these simulations, His12, Lys41, and His119 were treated as titratable. Long range electrostatics were computed using the smooth particle mesh Ewald (PME) method.[29,30] Note that the PME method implicitly introduces a background term that neutralizes the system (sometimes termed a "neutralizing plasma") that is further corrected for finite size effects[31] with a volume-dependent term. Other corrections can be made to remove pressure and free energy artifacts for charged periodic systems,[32] but in previous studies,[9] these were not found to be necessary and were not used here. Simulations were performed using a 2 fs integration step, with exchanges between adjacent replicas attempted every 200 fs, and conducted to 74 and 104 ns for each replica of apo and cCMP-bound RNase A. The 60 ns of production simulation was analyzed and reported for both systems. A full description of the simulation protocol, pH−activity curves, convergence tests on the sampled protonation states, and details about the side-chain conformations, hydrogen bonding networks in the active site, and binding of cCMP at different pH values can be found in the Supporting Information.

RESULTS AND DISCUSSION

Simulations Accurately Predict the Macroscopic pK_a Values for Apo and cCMP-Bound RNase A. Analysis of the pH-REMD simulations provides values for fractions $f_{(AH^+/B^-)}$, $f_{(AH^+/BH)}$, $f_{(A/BH)}$, and $f_{(A/B^-)}$ described in eqs 2−5, respectively, and, hence, via eqs 6 and 7 the overall acid and base fractions, $f_{(AH^+)}$ and $f_{(B^-)}$, respectively. The titration curves for His12, His119, and Lys41 for both apo and cCMP-complexed RNase A can be found in Figure 1. Each fraction is observed to exhibit

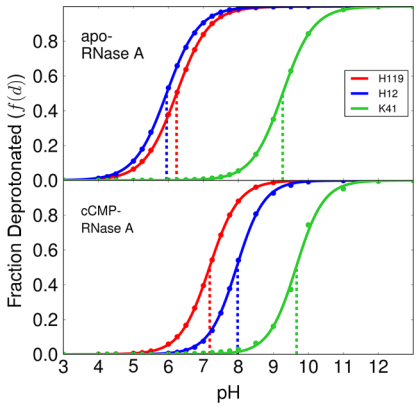

Figure 1. Titration curves (lines) fit to simulation data (points) with the Hill equation (eq 8). The top panel presents data for the apo enzyme and the bottom panel data for the cCMP-bound enzyme. The Hill coefficients for His119, His12, and Lys41 are 0.94, 0.94, and 0.98 for the apo enzyme and 1.04, 1.09, and 1.10 for the cCMP-bound enzyme, respectively.

near-ideal Henderson−Hasselbalch behavior. Fitting the acid and base fractions to the Hill equation (eq 8) allows direct evaluation of the simulated macroscopic pK_a values. A comparison of the simulated and experimental pK_a values is given in Table 1 for both apo and cCMP-complexed RNase A. In the case of apo RNase A, the simulated pK_a values for His12, His119, and Lys41 (5.95, 6.23, and 9.27, respectively) are within approximately 0.3 unit of the corresponding experimental values.[33,34] The simulations of RNase A complexed with cCMP predict pK_a values for His12, His119, and Lys41 shifted to 7.95, 7.17, and 9.65, respectively, in reasonable agreement with the experimentally estimated values of 8.0, 7.4, and 9.11, respectively.[34,35] In the course of the simulations over the pH range of 2−8, the integrity of the active site is maintained. Beyond pH 8, the interaction between Asp121 and His119 that form the His-Asp catalytic dyad begins to become displaced.[36] At high pH values, the cCMP becomes more loosely bound[37] in the binding pocket, leading to larger fluctuations and greater difficulty during sampling. Details

DOI: 10.1021/bi5012833
Biochemistry 2015, 54, 1307−1313

Table 1. Comparison of Experimental and Simulated Macroscopic pK_a Values for Apo and cCMP-Bound RNase A Using the Hill Equation (eq 8) and the "Apparent pK_a" Model[a]

	His12	His119	Lys41
apo RNase A			
exptl	5.8[b]	6.2[b]	9.0[c]
Hill equation	5.95 (0.14)	6.23 (0.07)	9.27 (0.07)
exptl ("apparent pK_a" estimate)[d]	4.9−5.2	6.3−6.9	–
"apparent pK_a model" with H12(B)/H119(A)	5.88 (0.14)	6.27 (0.08)	–
"apparent pK_a model" with K41(B)/H119(A)	–	6.17 (0.21)	8.81 (0.21)
cCMP-RNase A			
exptl (3′-CMP)	8.0[e]	7.4[e]	9.1[f]
Hill equation	7.95 (0.15)	7.17 (0.12)	9.65 (0.16)
exptl (cCMP "apparent pK_a")[g]	8.10	6.30	–
exptl (cCMP "apparent pK_a")[h]	9.0	6.25	–
"apparent pK_a model" with H119(B)/H12(A)	7.92 (0.16)	7.16 (0.12)	–
"apparent pK_a model" with H119(B)/K41(A)	–	7.18 (0.13)	9.64 (0.16)

[a]The calculated macroscopic pK_a values using the Hill equation (eq 8) and the "apparent pK_a model" for apo and cCMP-bound RNase A were compared with the experimental macroscopic and kinetic pK_a (exptl) values from the literature. Statistical error estimates, given in parentheses, were obtained as standard deviations derived from values computed from data in 5 ns intervals over the 60 ns of production. 3′-CMP and cCMP are the substrates 3′-cytidine monophosphate and 2′,3′-cyclic phosphate, respectively. [b]Taken from ref 33. [c]Taken from ref 34. [d]Range of values estimated from values reported in refs 21 and 39. [e]Taken from ref 35. [f]Taken from ref 34. [g]Taken from ref 38. [h]Taken from ref 19.

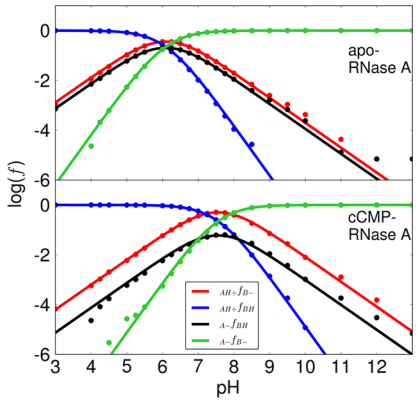

Figure 2. Microscopic pK_a model results with H12/H119 acting as the general acid/base. The plots of the logarithm of protonated fractions, log(f), vs pH of each microstate for apo (top) and cCMP-bound (bottom) RNase A were obtained by fitting the simulation data for all fractions to the equations derived from the microscopic model (Scheme 2) with His12/His119 acting as the general base/acid for apo RNase A (transphosphorylation model) and the general acid/base for cCMP-bound RNase A (hydrolysis model), respectively, as depicted in Scheme 1. The simulation data fits well with root-mean-square errors of 0.22 (apo) and 0.17 (cCMP) for the log(f) values. The log(f) maxima (−0.45 and −0.30, respectively) for the curve of the active fraction, $f_{(AH^+/B^-)}$, are 6.1 for the apo form and 7.5 for the cCMP form.

about the key structural features of the simulations at each pH are provided in the Supporting Information.

Simulated Protonation States Can Be Interpreted Using a Microscopic pK_a Model. The microscopic model illustrated in Scheme 2 was fit to the simulated fractions of His12 as the general base/acid and His119 as the general acid/base for apo and cCMP-bound RNase A (Figure 2). The model, which has three independent parameters, fits the simulation data extremely well. The general trend is that the curves for the cCMP complex shift to pH values higher than those for the apo enzyme. This trend is primarily due to the existence of the negatively charged cyclic phosphate on cCMP that is fairly close to the titratable residues in the active site. Further, the microscopic pK_a values derived from the fitting are in very good agreement with those measured from NMR experiments[36] for the apo enzyme (Table 2). For the cCMP-bound complex, to the best of our knowledge, experimental microscopic pK_a values that would allow a direct comparison currently do not exist. Nonetheless, there are microscopic pK_a values reported for a 3′-UMP inhibitor.[36] The microscopic pK_a values for His12 and His119 in the 3′-UMP-bound RNase A indicate a trend different from that of the experimental pK_a values for 3′-CMP- and cCMP-bound RNase A complexes[19,35,38] and the simulated values reported here (Table 1); nonetheless, we can compare the magnitude of the coupling (ΔpK_a values in Table 2) between protonation states.

The experimental microscopic pK_a values suggest that the His12 and His119 protonation states are weakly coupled in both the apo enzyme and the 3′-UMP-bound RNase A ($\Delta pK_{a,B}$ values of 0.31 and −0.1 pK_a unit, respectively). The calculated microscopic pK_a values are in reasonable agreement and predict the apo and cCMP-bound RNase A forms have $\Delta pK_{a,B}$ values of 0.17 and −0.21 pK_a unit, respectively. Overall, the experimental and calculated coupling between His12 and His119 protonation states is fairly weak. The observed weak coupling can be explained by the fact that the acid and base protonation sites are fairly far apart in the active site and, in the catalytically active state, involve interactions between a neutral and a positively charged residue (as opposed to oppositely charged residues). A fairly striking result is that the experimental $\Delta pK_{a,B}$ value for the 3′-UMP-bound RNase A is negative, suggesting that protonation of one of the active site histidine residues favors protonation of the other. This observation has been made experimentally[36] and has been explained as a result of enhanced interactions with the phosphate when both sites are protonated. The simulation results reported here are completely consistent with this interpretation (see the Supporting Information for additional details) and, as indicated in Table 2, suggest that only in the phosphate-bound systems does such cooperative coupling occur. The fact that the simulation results (for both the apo and cCMP complex enzymes) can be precisely fit to all four fractions by the three-parameter microscopic kinetic model lends credence to its validity.

The "Apparent" (uncorrelated) pK_a Model for His12/His119 Is Justified for the Catalytic Steps in RNase A. The experimental analysis of pH−rate data involves fitting the observed rate curve to a simple kinetic model with apparent pK_a values for the presumed general acid and base. The correspondence of directly measured macroscopic pK_a values of presumed general acid and base residues with the apparent pK_a

DOI: 10.1021/bi5012833
Biochemistry 2015, 54, 1307−1313

Table 2. Comparison of Experimental and Simulated Microscopic pK_a Values Using the Microscopic Model Illustrated in Scheme 2 for Apo and cCMP-Bound RNase A[a]

	$pK_{a,B}^{AH^+}$	$pK_{a,B}^{A}$	$\Delta pK_{a,B}$	$pK_{a,A}^{BH}$	$pK_{a,A}^{B^-}$	$\Delta pK_{a,A}$
apo RNase A with His12(B)/His119(A)						
exptl[b]	5.87	6.18	0.31	6.03	6.34	−0.31
microscopic model	5.88 (0.14)	6.05 (0.15)	0.17	6.13 (0.05)	6.30 (0.10)	−0.17
apo RNase A with Lys41(B)/His119(A)						
microscopic model	8.29 (0.14)	9.26 (0.07)	0.97	6.23 (0.07)	7.21 (0.21)	−0.97
cCMP-bound RNase A with His119(B)/His12(A)						
exptl (3′-UMP)[b]	7.95	7.85	−0.1	6.45	6.35	0.1
microscopic model	7.20 (0.12)	6.99 (0.20)	−0.21	8.12 (0.17)	7.92 (0.16)	0.21
cCMP-bound RNase A with His119(B)/Lys41(A)						
microscopic model	7.17 (0.12)	7.41 (0.40)	0.24	9.40 (0.18)	9.64 (0.16)	−0.24

[a]The calculated microscopic pK_a values are derived from the thermodynamic cycle illustrated in Scheme 2, which contains three free parameters that were fit to the acid/base fractions $f_{(AH^+/B^-)}$, $f_{(AH^+/BH)}$, $f_{(A/BH)}$, and $f_{(A/B^-)}$. The pK_a shifts are defined as $\Delta pK_{a,A} = pK_{a,A}^{BH} - pK_{a,A}^{B^-}$ and $\Delta pK_{a,B} = pK_{a,B}^{A} - pK_{a,B}^{AH^+}$. Note the constraint of the thermodynamic cycle in Scheme 2 ensures $\Delta pK_{a,A} + \Delta pK_{a,B} = 0$; a positive value for $\Delta pK_{a,B}$ indicates anticooperative coupling of protonation states (i.e., protonation of the acid site disfavors protonation of the base), whereas a negative value of $\Delta pK_{a,B}$ indicates cooperative coupling (i.e., protonation of the acid site favors protonation of the base). Statistical error estimates, given in parentheses, were obtained as standard deviations derived from values computed from data in 5 ns intervals over the 60 ns of production. Results were compared with the experimental (exptl) values obtained by NMR. [b]Taken from ref 36 to validate the model. In order to explore the degree to which this weak coupling persists with other plausible general base/acid pairs, the general base/acid was replaced with Lys41 for each case and the resulting microscopic pK_a values were determined.

values is often interpreted as indirect evidence that supports their catalytic roles. The computational analogue of this procedure would be to fit only the active fraction, $f_{(AH^+/B^-)}$, to the thermodynamic cycle shown in Scheme 2, but with only two free parameters, p$K_{a,A}$ and p$K_{a,B}$ (or, alternatively, under constraints that $pK_{a,A}^{B^-} = pK_{a,A}^{BH}$ and $pK_{a,B}^{AH^+} = pK_{a,B}^{A}$). The fitted apparent p$K_a$ curve for His12 and His119 as the general acid and base, respectively, is shown in Figure 3, and the apparent pK_a values are listed in Table 1. Note that although the apparent pK_a values consider only the active fraction in the fitting, as would be the procedure used to fit experimental curves, these parameters also determine the fractions of the other protonation states in accord with the partition function in eq 1. Unlike experiment, these nonactive fractions are available from the simulations, and thus available for comparison. The fit to the active fraction (red line in Figure 3) is excellent; however, model curves for the other fractions, particularly $f_{(A^-/BH)}$, are somewhat worse than for the curves shown in Figure 2 that involved fitting the microscopic model to all of the fractions simultaneously. Nonetheless, the apparent pK_a values fit to the active fraction are in remarkably close agreement (within 0.07 pK_a unit) with the macroscopic pK_a values that were derived from fitting the protonation fractions to the Hill equation (Table 1). This is a direct consequence of the very weak coupling between the His12 and His119 protonation states. Under these conditions, the assumptions of independent protonation events and the interpretation of the apparent pK_a values used to gain insight into the general acid−base mechanism are valid. Note, however, the present discussion assumes that the only protonation events that are affecting the catalytic activity are those of the general acid and base, and in many cases, this may not be true.

Coupling of Protonation States for His119 and Lys41 Is Significant. Our example of general acid−base catalysis in apo RNase A, with His12 and His119 as the presumed general acid and base, respectively, indicates that treatment of the protonation states as uncorrelated within the framework of the "apparent pK_a model" is justified. However, it should not be assumed that this is a general phenomenon. To demonstrate

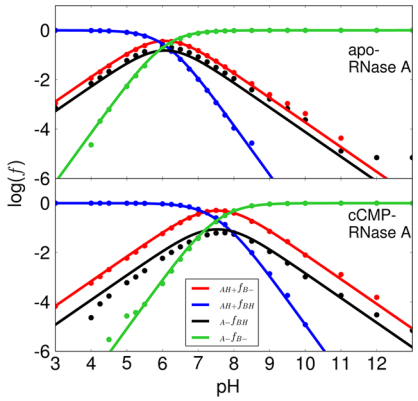

Figure 3. Apparent pK_a model results with H12/H119 acting as the general acid and base. The plots of the protonated fractions, log(f), vs pH of each microstate for apo (top) and cCMP-bound RNase A (bottom) were obtained by fitting the simulation data to only the active fraction [$f_{(AH^+/B^-)}$, colored red] with His12/His119 acting as the general base/acid for apo RNase A (transphosphorylation model) and the general acid/base for cCMP-bound RNase A (hydrolysis model), respectively, as depicted in Scheme 1. The model assumes no coupling of the microstates, and although only the active fraction is considered in the fitting (as would be the case experimentally), the parameters nonetheless are able to determine the other fractions that can be compared with the simulation data. The top panel shows data for the apo RNase A and the bottom panel data for the cCMP-bound RNase A. The root-mean-square errors for the log(f) values are 0.25 for the apo form and 0.18 for the cCMP-bound form. The log(f) maxima (−0.43 and −0.30, respectively) for the curve of the active fraction, $f_{(AH^+/B^-)}$, are at 6.1 for the apo form and 7.5 for the cCMP-bound form.

this point, we consider the scenario whereby the role of the general base is replaced by Lys41 in the kinetic model for the apo RNase A enzyme. Evidence suggests this is likely not the biological role of Lys41 in catalysis by RNase A, but for the purposes of demonstration, it is still instructive to examine.

The microscopic model is able to fit the simulation data very well for all fractions (Figure 4). However, considerably stronger protonation state coupling ($\Delta pK_{a,A} = \Delta pK_{a,B} = 0.97$) is

DOI: 10.1021/bi5012833
Biochemistry 2015, 54, 1307−1313

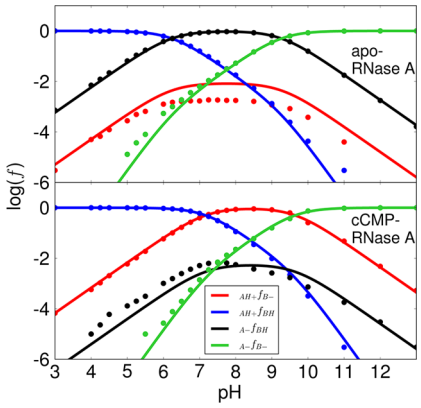

Figure 4. Microscopic pK_a model results with K41/H119 acting as the general acid and base. The plots of the logarithm of protonated fractions, log(f), vs pH of each microstate for apo (top) and cCMP-bound RNase A (bottom) were obtained by fitting the simulation data for all fractions to the equations derived from the microscopic model (Scheme 2) with Lys41/His119 acting as the general base/acid for apo RNase A (transphosphorylation model) and the general acid/base for cCMP-bound RNase A (hydrolysis model), respectively. This is not the generally accepted mechanism depicted in Scheme 1 but has nonetheless received some support in the literature[24,40] and so is considered here for comparison. The root-mean-square errors for the log(f) values are 0.31 for the apo form and 0.44 for the cCMP-bound form. The log(f) maxima (−2.09 and −0.05, respectively) for the curve of the active fraction, $f_{(AH^+/B^-)}$, are 7.7 for the apo form and 8.4 for the cCMP-bound form.

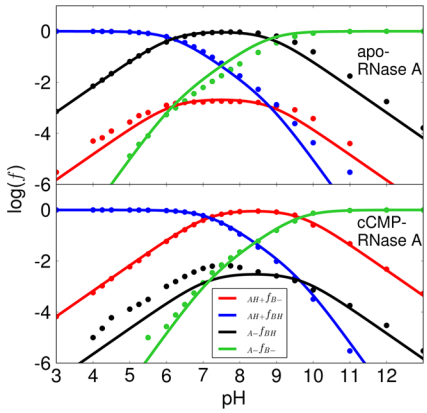

Figure 5. Apparent pK_a model results with K41/H119 acting as the general acid and base. The plots of the logarithm of protonated fractions, log(f), vs pH of each microstate for apo (top) and cCMP-bound RNase A (bottom) were obtained by fitting the simulation data to only the active fraction [$f_{(AH^+/B^-)}$, colored red] with Lys41/His119 acting as the general base/acid for apo RNase A (transphosphorylation model) and the general acid/base for cCMP-bound RNase A (hydrolysis model), respectively. This is not the generally accepted mechanism depicted in Scheme 1 but has nonetheless received some support in the literature[24,40] and so is considered here for comparison. The model assumes no coupling of the microstates, and although only the active fraction is considered in the fitting (as would be the case experimentally), the parameters nonetheless are able to determine the other fractions that can be compared with the simulation data. The top panel shows data for apo RNase A and the bottom panel data for cCMP-bound RNase A. The root-mean-square errors for the log(f) values are 0.33 for the apo form and 0.48 for the cCMP-bound form. The log(f) maxima (−2.69 and −0.11, respectively) for the curve of the active fraction, $f_{(AH^+/B^-)}$, are 7.5 for the apo form and 8.4 for the cCMP-bound form.

observed between Lys41 and His119 than between His12 and His119 (Table 2). The apparent pK_a values for Lys41 and His119 are 8.81 and 6.17, respectively, which differ somewhat from the macroscopic pK_a values obtained from the Hill equation (9.27 and 6.23, respectively). Moreover, the "apparent pK_a model" does not closely reproduce the protonation state fractions (Figure 5), including the active fraction that was used in the fitting. Although the slopes of the higher- and lower-pH regimes of the pH−rate curve are not influenced by the interactions between the residues, the maximal probability is observed to be approximately 3 times larger. However, the predicted pK_a from the microscopic model illustrates that the "apparent pK_a model" has limitations with regard to mechanistic interpretation in the regime where key protonation states are more strongly coupled. This may be particularly relevant for some RNA enzymes in which the active forms of the general acid and base are oppositely charged species that can be expected to exhibit stronger electrostatic interactions.

Summary and Perspective. Recently, advances in computational methods have allowed simulations of biological molecules to be performed in explicit solvent under constant pH conditions. These simulations allow conformations and protonation states to be sampled together across a range of pH conditions. This allows the prediction of pH−rate curves from molecular simulation and provides tools for providing atomic-level interpretation of pH−activity data. More importantly, this method allows one to quantify the probability of finding an enzyme system in a catalytically active protonation state from which it is capable of going on to react with a pseudo-first-order rate constant in the catalytic chemical step. Together with other methods, such as combined quantum mechanical/molecular mechanical simulations that can be used to map the free energy landscape for the catalytic chemical steps of the reaction, a complete description of catalysis can be obtained and compared directly with experimental data. The results described here demonstrate promise for theory and experiment to work together to improve our understanding of enzyme mechanisms.

■ ASSOCIATED CONTENT

Supporting Information

A full description of the simulation protocol, pH−activity curves, convergence tests on the sampled protonation states, and details about the side-chain conformations, hydrogen bonding networks in the active site, and binding of cCMP at different pH values. This material is available free of charge via the Internet at http://pubs.acs.org.

■ AUTHOR INFORMATION

Corresponding Author

*E-mail: york@biomaps.rutgers.edu.

Funding

This work was financially supported by National Institutes of Health (NIH) Grant GM062248 to D.M.Y., NIH Grant GM096000 to M.E.H., and National Science Foundation (NSF) Grants ACI-1147910 and ACI-1036208 to A.E.R. The simulations were conducted with the Blue Waters supercomputer, supported by NSF Grants ACI-0725070 and ACI-1238993, and the Extreme Science and Engineering Discovery Environment (XSEDE), supported by NSF Grant OCI-1053575.

Notes

The authors declare no competing financial interest.

DOI: 10.1021/bi5012833
Biochemistry 2015, 54, 1307−1313

■ ACKNOWLEDGMENTS

Special thanks to Timothy Giese, Ming Huang, and Maria Panteva for their for useful suggestions about the manuscript.

■ REFERENCES

(1) Kirby, A. J. (2010) Acid-Base Catalayis by Enzymes. *Encyclopedia of Life Sciences (ELS)*, John Wiley & Sons, Ltd., Chichester, U.K.
(2) Raines, R. T. (1998) Ribonuclease A. *Chem. Rev. 98*, 1045−1065.
(3) Cuchillo, C. M., Nogués, M. V., and Raines, R. T. (2011) Bovine pancreatic ribonuclease: Fifty years of the first enzymatic reaction mechanism. *Biochemistry 50*, 7835−7841.
(4) Doudna, J. A., and Cech, T. R. (2002) The chemical repertoire of natural ribozymes. *Nature 418*, 222−228.
(5) Onufriev, A., Case, D. A., and Ullmann, G. M. (2001) A novel view of pH titration in biomolecules. *Biochemistry 40*, 3413−3419.
(6) Bevilacqua, P. C. (2003) Mechanistic considerations for general acid-base catalysis by RNA: Revisiting the mechanism of the hairpin ribozyme. *Biochemistry 42*, 2259−2265.
(7) Ullmann, G. M. (2003) Relations between protonation constants and titration curves in polyprotic acids: A critical view. *J. Phys. Chem. B 107*, 1263−1271.
(8) Klingen, A. R., Bombarda, E., and Ullmann, G. M. (2006) Theoretical investigation of the behavior of titratable groups in proteins. *Photochem. Photobiol. Sci. 5*, 588−596.
(9) Swails, J. M., York, D. M., and Roitberg, A. E. (2014) Constant pH replica exchange molecular dynamics in explicit solvent using discrete protonation states: Implementation, testing, and validation. *J. Chem. Theory Comput. 10*, 1341−1352.
(10) Wallace, J. A., and Shen, J. K. (2011) Continuous constant pH molecular dynamics in explicit solvent with pH-based replica exchange. *J. Chem. Theory Comput. 7*, 2617−2629.
(11) Wallace, J. A., and Shen, J. K. (2012) Charge-leveling and proper treatment of long-range electrostatics in all-atom molecular dynamics at constant pH. *J. Chem. Phys. 137*, 184105.
(12) Goh, G. B., Knight, J. L., and Brooks, C. L. (2012) Constant pH molecular dynamics simulations of nucleic acids in explicit solvent. *J. Chem. Theory Comput. 8*, 36−46.
(13) Goh, G. B., Knight, J. L., and Brooks, C. L., III (2013) pH-dependent dynamics of complex RNA macromolecules. *J. Chem. Theory Comput. 9*, 935−943.
(14) Baptista, A. M., Teixeira, V. H., and Soares, C. M. (2002) Constant-pH molecular dynamics using stochastic titration. *J. Chem. Phys. 117*, 4184−4200.
(15) Donnini, S., Tegeler, F., Groenhof, G., and Grubmüller, H. (2011) Constant pH molecular dynamics in explicit solvent with λ-dynamics. *J. Chem. Theory Comput. 7*, 1962−1978.
(16) Börjesson, U., and Hünenberger, P. H. (2001) Explicit-solvent molecular dynamics simulation at constant pH: Methodology and application to small amines. *J. Chem. Phys. 114*, 9706−9719.
(17) Itoh, S. G., Damjanović, A., and Brooks, B. R. (2011) pH replica-exchange method based on discrete protonation states. *Proteins 79*, 3420−3436.
(18) Findlay, D., Mathias, A. P., and Rabin, B. R. (1962) The active site and mechanism of action of bovine pancreatic ribonuclease. 4. The activity in inert organic solvents and alcohols. *Biochem. J. 85*, 134−138.
(19) Eftink, M. R., and Biltonen, R. L. (1983) Energetics of ribonuclease A catalysis. 1. pH, ionic strength, and solvent isotope dependence of the hydrolysis of cytidine cyclic 2′,3′-phosphate. *Biochemistry 22*, 5123−5134.
(20) Park, C., Schultz, L. W., and Raines, R. T. (2001) Contribution of the active site histidine residues of ribonuclease A to nucleic acid binding. *Biochemistry 40*, 4949−4956.
(21) Park, C., and Raines, R. T. (2003) Catalysis by ribonuclease A is limited by the rate of substrate association. *Biochemistry 42*, 3509−3518.
(22) Kim, M. O., Blachly, P. G., Kaus, J. W., and McCammon, J. A. (2015) Protocols utilizing constant pH molecular dynamics to compute pH-dependent binding free energies. *J. Phys. Chem. B 119*, 861−872.
(23) Wladkowski, B. D., Krauss, M., and Stevens, W. J. (1995) Ribonuclease A catalyzed transphosphorylation: An *ab initio* theoretical study. *J. Phys. Chem. 99*, 6273−6276.
(24) Wladkowski, B. D., Ostazeski, P., Chenoweth, S., Broadwater, S. J., and Krauss, M. (2003) Hydrolysis of cyclic phosphates by ribonuclease A: A computational study using a simplified ab initio quantum model. *J. Comput. Chem. 24*, 1803−1811.
(25) Berisio, R., Sica, F., Lamzin, V. S., Wilson, K. S., Zagari, A., and Mazzarella, L. (2002) Atomic resolution structures of ribonuclease A at six pH values. *Acta Crystallogr. D58*, 441−450.
(26) Zegers, I., Maes, D., Dao-Thi, M.-H., Poortmans, F., Palmer, R., and Wyns, L. (1994) The structures of RNase A complexed with 3′-CMP and d(CpA): Active site conformation and conserved water molecules. *Protein Sci. 3*, 2322−2339.
(27) Case, D. A., et al. (2012) *AMBER 12*, University of California, San Francisco, San Francisco.
(28) Horn, H. W., Swope, W. C., Pitera, J. W., Madura, J. D., Dick, T. J., Hura, G. L., and Head-Gordon, T. (2004) Development of an improved four-site water model for biomolecular simulations: TIP4P-Ew. *J. Chem. Phys. 120*, 9665−9678.
(29) Darden, T., York, D., and Pedersen, L. (1993) Particle mesh Ewald: An N log(N) method for Ewald sums in large systems. *J. Chem. Phys. 98*, 10089−10092.
(30) Essmann, U., Perera, L., Berkowitz, M. L., Darden, T., Hsing, L., and Pedersen, L. G. (1995) A smooth particle mesh Ewald method. *J. Chem. Phys. 103*, 8577−8593.
(31) Figueirido, F., Del Buono, G. S., and Levy, R. M. (1995) On finite-size effects in computer simulations using the Ewald potential. *J. Chem. Phys. 103*, 6133−6142.
(32) Bogusz, S., Cheatham, T. E., III, and Brooks, B. R. (1998) Removal of pressure and free energy artifacts in charged periodic systems via net charge corrections to the Ewald potential. *J. Chem. Phys. 108*, 7070−7084.
(33) Markley, J. L. (1975) Correlation proton magnetic resonance studies at 250 MHz of bovine pancreatic ribonuclease. I. Reinvestigation of the histidine peak assignments. *Biochemistry 14*, 3546−3554.
(34) Jentoft, J., Gerken, T., Jentoft, N., and Dearborn, D. (1981) [^{13}C]Methylated Ribonuclease A, ^{13}C NMR studies of the interaction of lysine 41 with active site ligands. *J. Biol. Chem. 256*, 231−236.
(35) Meadows, D. H., and Jardetzky, O. (1968) Nuclear magnetic resonance studies of the structure and binding sites of enzymes. IV. Cytidine 3′-monophosphate binding to ribonuclease. *Proc. Natl. Acad. Sci. U.S.A. 13*, 406−413.
(36) Quirk, D. J., and Raines, R. T. (1999) His···Asp catalytic dyad of ribonuclease A: Histidine pK_a values in the wild-type, D121N, and D121A enzymes. *Biophys. J. 76*, 1571−1579.
(37) Neuberger, A., and Brocklehurst, K., Eds. (1987) *Hydrolytic Enzymes. New Comprehensive Biochemistry*, Elsevier, Amsterdam.
(38) Herries, D., Mathias, A. P., and Rabin, B. R. (1962) The active site and mechanism of action of bovine pancreatic ribonuclease. 3. The pH-dependence of the kinetic parameters for the hydrolysis of cytidine 2′,3′-phosphate. *Biochem. J. 85*, 127−134.
(39) Gu, H., Zhang, S., Wong, K.-Y., Radak, B. K., Dissanayake, T., Kellerman, D. L., Dai, Q., Miyagi, M., Anderson, V. E., York, D. M., Piccirilli, J. A., and Harris, M. E. (2013) Experimental and computational analysis of the transition state for ribonuclease A-catalyzed RNA 2′-*O*-transphosphorylation. *Proc. Natl. Acad. Sci. U.S.A. 110*, 13002−13007.
(40) Wladkowski, B. D., Krauss, M., and Stevens, W. J. (1995) Transphosphorylation catalyzed by ribonuclease A: Computational study using *ab initio* effective fragment potentials. *J. Am. Chem. Soc. 117*, 10537−10545.

DOI: 10.1021/bi5012833
Biochemistry 2015, 54, 1307−1313